We are IntechOpen,
the world's leading publisher of
Open Access books
Built by scientists, for scientists

6,900
Open access books available

185,000
International authors and editors

200M
Downloads

154
Countries delivered to

Our authors are among the

TOP 1%
most cited scientists

12.2%
Contributors from top 500 universities

BOOK CITATION INDEX INDEXED
CLARIVATE ANALYTICS

WEB OF SCIENCE™

Selection of our books indexed in the Book Citation Index
in Web of Science™ Core Collection (BKCI)

Interested in publishing with us?
Contact book.department@intechopen.com

Numbers displayed above are based on latest data collected.
For more information visit www.intechopen.com

15

High-Temporal Global Rainfall Maps from Satellite Passive Microwave Radiometers

Shoichi Shige
Kyoto University
Japan
Satoshi Kida & Tomoya Yamamoto
Osaka Prefecture University
Japan
Takuji Kubota
Japan Aerospace Exploration Agency
Japan
Kazumasa Aonashi
Meteorological Research Institute
Japan

1. Introduction

High-precision and high-temporal global rainfall maps are very important for scientific studies for global water cycle and practical applications for water resources. However, rainfall has been poorly measured by ground-based observations. In particular, very few in situ measurements of rainfall are available for over the oceans owing to sparse observations. Therefore, satellite remote sensing is the only way to measure rainfall globally. Historically, the earliest satellite observations of the Earth were made in the visible and infrared regions. Therefore, cloud-top temperature and cloud patterns from visible and infrared radiometers had been used to estimate rainfall globally based on an empirical relationship with ground-level rain rate (e.g. Arkin & Meisner 1987).

A more direct measure of rainfall can be obtained using passive microwave radiometers (MWRs) because its ability to penetrate clouds and measure the emitted radiation from rainwater and the scattering caused by cloud ice and snow. During the past three decades, passive MWRs have evolved from single-channel radiometers with low spatial resolution such as the Electronically Scanning Microwave Radiometer (ESMR) on Nimbus-5 to higher-resolution sensors with many channels such as the Advanced Microwave Scanning Radiometer for the Earth Observing System (AMSR-E; Kawanishi et al. 2003) aboard the *Aqua* satellite. Since the launch of the first Special Sensor Microwave Imager (SSM/I; Hollinger et al. 1990; Colton & Poe 1999) on the Defense Meteorological Satellite Program (DMSP), passive MWRs have been a standard instrument in global rainfall retrieval. The problems of passive MWR rainfall retrieval algorithms lie in the fact they are not fully constrained. Since brightness temperatures (Tbs) measured by

passive MWRs are the end product of the integrated effects of electromagnetic absorption/emission and scattering through a precipitating cloud along the sensor viewpath, a priori model or database for the three-dimensional (3D) properties of precipitating clouds are required to establish relationship between Tbs and rain rates.

A new age of active microwave remote sensing of precipitation from space began with the launch of the Tropical Rainfall Measuring Mission (TRMM; Simpson et al. 1988, 1996) which carries the first space-borne radar (Precipitation Radar (PR); Kozu et al. 2001; Okamoto 2003; Okamoto & Shige 2008) together with the TRMM Microwave Imager (TMI; Kummerow et al. 1998). The PR has enabled us to directly obtain vertical profiles of precipitation over the global Tropics (Iguchi 2007; Iguchi et al. 2000, 2009). Information obtained by the TRMM PR accelerated the development of passive MWR rainfall retrieval algorithms (Viltard et al. 2006; Kummerow et al. 2007). One algorithm using precipitation-related variable models and retrieval methods based on TRMM observation studies is the Global Satellite Mapping of Precipitation (GSMaP) algorithm (Aonashi et al. 2009; Kubota et al. 2007). The GSMaP algorithm has been applied to MWRs currently in orbit such as SSM/I, TMI, and AMSR-E to produce global precipitation maps. Despite the improved rainfall estimates using data from passive MWRs, the challenge remains to further fill information gaps through more frequent satellite observations. Passive MWRs are generally of two types: imagers and sounders. Microwave imagers (MWIs) such as the SSM/I, TMI and AMSR-E, and have channels suitable for monitoring precipitation. Microwave sounders (MWSs) such as the Advanced Microwave Sounding Unit (AMSU) (Mo 1996; Saunders et al. 1995) aboard the National Oceanic and Atmospheric Administration (NOAA) satellites and the first satellite of the Meteorological Operational satellite program (MetOp-A) are primarily developed for profiling atmospheric temperature and moisture using opaque spectral regions. Two AMSU-based rainfall retrieval algorithms have been developed. One is a neural-network-based algorithm developed at the Massachusetts Institute of Technology, Cambridge (Surussavadee & Staelin 2008a,b). The algorithm is trained using a cloud-resolving model. The other is the Microwave Surface and Precipitation Products System (MSPPS) Day-2 rainfall algorithm for the AMSU and has been developed at NOAA (Ferraro et al. 2005).

Because there have been four AMSU instruments in orbit since the launch of NOAA18 in 2005, together with five MWIs (TMI, AMSR-E, and SSM/I), there have been more observations of rainfall in time and space, with swaths being ~2200 km wide. Another advantage of the four AMSU sensors on the NOAA satellites and MetOp-A is that they are typically spaced about 4 h in time, thus giving a better representation of the diurnal cycle.

Kubota et al. (2009) demonstrated effective performance of the merger of the MWSs in addition to the MWIs by the ground-radar validation around Japan. However, the multitude of satellite data sources does not come without its problem. Bias errors in the retrieved rain rates that vary between MWIs and MWSs are troublesome for many applications. The only way to try to overcome this problem is to develop a consensus algorithm applicable to both MWIs and MWSs based on the same physical principle. Recently, Shige et al. (2009) developed an over-ocean rainfall retrieval algorithm for MWS (GSMaP_MWS) that shares at a maximum a common algorithm framework with the GSMaP algorithm for MWI (GSMaP_MWI; Aonashi et al. 2009; Kubota et al. 2007). The purpose of this paper is to briefly describe GSMaP_MWS algorithm and provide examples of rainfall maps from MWRs (MWIs + MWSs).

2. Overview of retrieval algorithm

A flowchart of the GSMaP_MWI and GSMaP_MWS algorithms is shown in Fig. 1. Here, the TMI version of GSMaP_MWI (GSMaP_TMI) and the AMSU version of GSMaP_MWS (GSMaP_AMSU) are described. Similar to the GSMaP_MWI algorithm, the GSMaP_MWS algorithm consists of two parts: the forward calculations for making the lookup tables (LUTs) showing the relationship between rainfall rates and Tbs with a radiative transfer model (RTM), and the retrieval part to estimate precipitation rates from the observed Tbs using the LUTs. The GSMaP_MWS algorithm shares information required for the RTM calculation with the GSMaP_MWI algorithm. Also in the retrieval process, the GSMaP_MWS algorithm retains the basic structure of the GSMaP_MWI algorithm.

2.1 Forward calculation

The RTM calculation requires information on atmospheric variables, as well as precipitation-related variables. Atmospheric temperature, freezing-level height (FLH), surface winds, and surface temperature are adapted from the Japan Meteorological Agency (JMA) global analysis (GANAL). Similarly, sea surface temperature is adapted from JMA merged satellite and *in situ* data global daily sea surface temperatures in the global ocean. As for relative humidity, the constant value of 100% is assumed.

The convective and stratiform precipitation models for precipitation-related variables (hydrometer profiles, drop-size distribution (DSD), etc.) are constructed for ten precipitation types. Precipitation types are determined in terms of stratiform pixel ratio, stratiform rain ratio, precipitation area, precipitation top height, rain intensity, and diurnal cycle from the PR data, together with the ratio between PR precipitation rates and TRMM lightning imaging sensor flash rates (Takayabu & Katayama 2004: Takayabu 2006, 2008). Precipitation types consist of six land types (severe thunderstorm, afternoon shower, shallow convection, extratropical cyclone, organized convection, and highland rain) and four ocean types (shallow convection, extratropical cyclone, transition zone, and organized convection). Global distributions of the precipitation types in 2.5° × 2.5° latitude–longitude boxes are statistically classified trimonthly.

The convective and stratiform precipitation profiles of PR data are averaged over prescribed precipitation ranges for each precipitation type. In this averaging, profiles relative to FLH are used to exclude the influence of atmospheric temperature variations (Kubota et al. 2007). The database of precipitation types and profiles makes it possible for the algorithm to deal with trimonthly variation of typical hydrometeor profiles.

For rain DSD, a gamma distribution of rain drop size is assumed:

$$N(D) = N_0 D^\mu \exp(-\Lambda D) \qquad (1)$$

where $N(D)$ is the number concentration for particles with diameter D, $\mu=3$, N_0 and Λ are parameters to be determined. For convective precipitation, N_0 and Λ are determined using DSD parameter estimated from the ''α-adjustment'' method of PR algorithm (Kozu et al. 2009). For stratiform precipitation, the standard values of N_0 and Λ assumed in PR algorithm is used.

On the other hand, conventional models were used for frozen and mixed-phase particle-size distribution that could not be estimated from the TRMM PR observation. The exponential distribution is used for the DSD model of snow and graupel. The refractivity of convective

and stratiform frozen particles is calculated, assuming them as the mixture of ice and air with an empirically prescribed constant density (200 kg m⁻³). Particle-size distribution and refractivity for mixed-phase stratiform precipitation (between FLH minus 1 km and FLH) were parameterized in terms of atmospheric temperature (Nishitsuji et al. 1983; Takahashi & Awaka 2005), while mixed-phase convective precipitation was neglected.
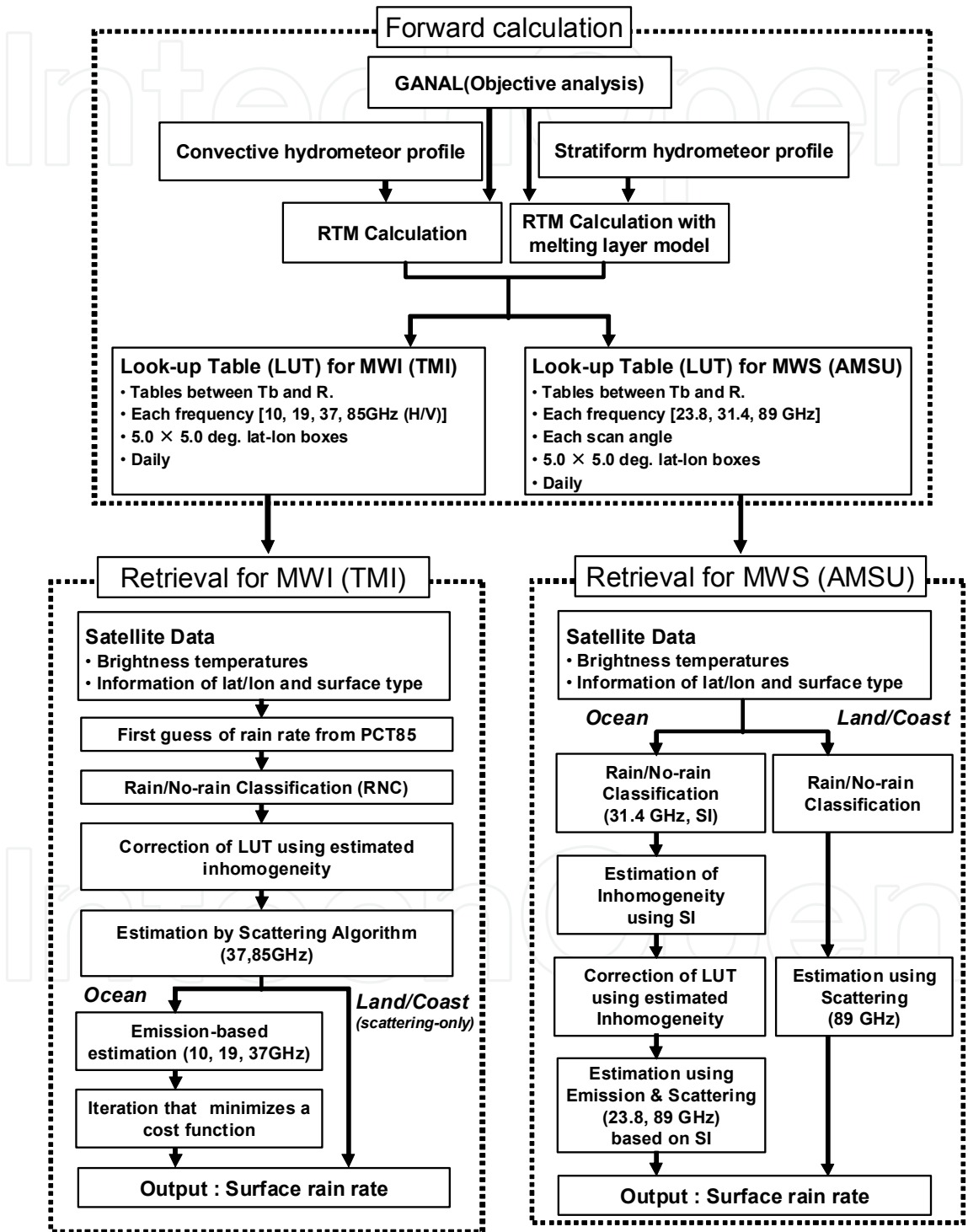

Fig. 1. Flowchart for the GSMaP algorithm for microwave imager (MWI) and microwave sounder (MWS)

From forward calculations with a four-stream RTM (Liu 1998), LUTs showing the relationship between rainfall rates and Tbs were computed daily in $5.0° \times 5.0°$ latitude–longitude boxes. While conical scanning radiometers such as the TMI preferentially scan at a constant slant path angle, the AMSU radiometer uses cross-track scanning to view the Earth. The variations in path lengths through which the atmosphere is viewed by cross-track scanning should be taken into account. For the AMSU, the received polarization also varies with scan angle because of the rotating-reflector/fixed-feed horn antenna design. This is different from that of imagers using a conical scanning mechanism, which receive a fixed polarization independent of the scan. At a given scan angle θ_s, the normalized surface emitted radiation (i.e., emissivity) ε_s seen by the AMSU contains mixed vertical ε_V and horizontal ε_H polarizations (the very small cross-polarized contribution due to imperfect cross-polarization isolation in the antenna is neglected), i.e.,

$$\varepsilon_s = \varepsilon_V(\theta) \cos 2\theta_s + \varepsilon_H(\theta) \sin 2\theta_s \qquad (2)$$

where the local zenith angle θ (LZA) varies as a function of scan angle θ_s (Grody et al. 2001). The LUTs are produced for each scan angle from RTM calculations using (2). For a sea surface, the emissivity components ε_V and ε_H are calculated using the Fresnel formula for calm seas (Guillou et al. 1998), together with an empirical model that includes the effects of wind-driven foam and surface roughness on emissivity (Schluessel & Luthardt 1991), while for a land surface, they are set at 0.9.

2.2 Retrieval

The retrieval process of the GSMaP_MWS has been developed, retaining the basic structure of the GSMaP_MWI algorithm. Emission signatures are mainly used to determine rainfall, while scattering signatures are used to help define the nature of precipitation. Taking advantage of 150 GHz of AMSU, an SI is defined as follows:

$$\text{SI} = (\text{Tb89} - \text{Tb89}_{LUT0}) - (\text{Tb150} - \text{Tb150}_{LUT0}). \qquad (3)$$

where Tb89_{LUT0} and Tb150_{LUT0} are Tb89 and Tb150 at 0 mm h^{-1} in the LUTs, respectively. Because the response to snow and graupel lowers the Tb and increases strongly with frequency, the Tb reduction is higher at 150 GHz than at 89 GHz. Thickness between precipitation top height and freezing level height increases with AMSU-B SI (Fig. 6 of Shige et al. 2009). In the retrieval process, SI is used as a key parameter.

Similar to the GSMaP_MWI algorithm, rain or no-rain flags are identified by deterministic methods at the beginning of this process. Then, the horizontal inhomogenity of rainfall within rather large AMSU FOVs is taken into account by the algorithm in order to properly compensate for nonlinearities in the Tbs versus water content relationships. The LUTs at 23 GHz and 89 GHz are corrected using the horizontal inhomogenity of rainfall estimated from SI for AMSU-A and AMSU-B FOVs, respectively. Using the corrected LUTs, rain rates are retrieved from Tb23 and Tb89, and these estimates are combined depending SI to give the rainfall estimate at AMSU-B FOV.

3. Results

3.1 The matched TRMM and NOAA-15(NK) case

In principle, rainfall retrievals using data from the PR and TMI aboard the TRMM satellite are superior to those using data from AMSU instruments, which have coarser FOVs and channels for profiling atmospheric temperature and moisture instead of precipitation. The PR provides height information based upon the time delay of the precipitation-backscattered return power and allows vertical profiles of precipitation to be obtained directly. The TMI is equipped with channels suitable for monitoring precipitation; in particular, 10 GHz channel has nearly linear relationship between rainfall rates and Tbs. Thus, a comparison of AMSU estimates against TRMM estimates is very useful for the development and validation of AMSU rainfall retrievals.

Figure 2 shows rain-rate maps from PR, GSMaP_TMI, and GSMaP_AMSU for the matched TRMM and NOAA-15(NK) case on 25 July 2005 over Atlantic Ocean, together with that from the Microwave Surface and Precipitation Products System (MSPPS) Day-2 rainfall algorithm for the AMSU. The MSPPS Day-2 rainfall algorithm for the AMSU (hereinafter NOAA_AMSU) was developed at NOAA (Ferraro et al. 2005). A simultaneous retrieval of the ice water path (IWP) and ice-particle effective diameter (De) from Tb data at 89 and 150 GHz was performed through two processes: simplifying the radiative transfer equation into a two-stream approximation and estimating the cloud-base and cloud-top Tbs through the use of AMSU measurements at 23.8 and 31.4 GHz. The rain rate was computed based on an IWP and rain-rate relation derived from the GPROF algorithm database, which contains the profiles of various hydrometeors generated from the cloud-resolving models. The weakness of the NOAA_AMSU algorithm was that only precipitation that is detectable from a scattering signature can be estimated (Huffman et al. 2007, Joyce et al. 2004). Recently, a new correction has been developed for the AMSU-A cloud liquid water content to fill in the gaps of NOAA_AMSU retrievals over ocean (Vila et al. 2007). Rain estimates shown in Fig. 2 d were derived using the improved NOAA_AMSU algorithm.

It can be seen with AMSU has much wider swath (~2200 km; Fig. 2c, d) than PR (~220 km; Fig. 2a) and TMI (~760 km; Fig. 2b), giving more observation of rainfall in time and space. Both GSMaP_AMSU and NOAA_AMSU depict similar large-scale structure with PR and GSMaP_TMI. However, there is considerable disagreement between GSMaP_AMSU and NOAA_AMSU at the finescale. GSMaP_AMSU detects scattered rain pixels, while NOAA_AMSU does not. The rain/no-rain classification method in GSMaP_AMSU uses not only the AMSU-A data but also SI from the AMSU-B data, leading to detection of scattered rain pixels.

3.2 Combined microwave estimates

Figure 3 shows combined precipitation estimate for the 3-h period from MWIs (SSM/I on three DMSP satellites, TMI on TRMM and AMSR-E on *Aqua*). The coverage of these MWIs is about 60 % of the earth's surface in the latitude band 60oN-S. On the other hand, Fig. 4 shows combined precipitation estimate for the 3-h period from passive MWIs and MWSs (i.e. AMSU). The addition of AMSU allows for better coverage (about 90 %), thus adding improved global rainfall retrieval. The data voids in the latitude band 45oS-60oS arise not from the lack of the data from MWIs and MWSs, but from unfavorable condition. The

current GSMaP algorithm mask sea ice regions where rain retrievals are not possible using AMSR-E Sea Ice Concentration product (Comiso 2009).

Combined precipitation estimate for the 3-h period from MWIs and MWRs has been obtained by Joyce et al. (2004) and Huffman et al. (2007; their Fig. 1). Different precipitation retrieval algorithms were applied to MWIs and MWSs. For example, in the study of Huffman et al. (2007), passive microwave FOVs from the TMI, AMSR-E, and SSM/I were converted to precipitation estimates with the Goddard Profiling Algorithm (GPROF) (Kummrow et al. 1996, 2001; Olson et al. 2006; Wilheit et al. 2003), while those from AMSU were converted to precipitation estimates with the NOAA_AMSU algorithm (Ferraro et al. 2005). The primary difference from the previous studies is that the combined precipitation estimate shown in Fig. 4 is deduced from the algorithms for MWIs and MWSs that share information required for the RTM calculation and the basic structure of retrieval process (Fig. 1).
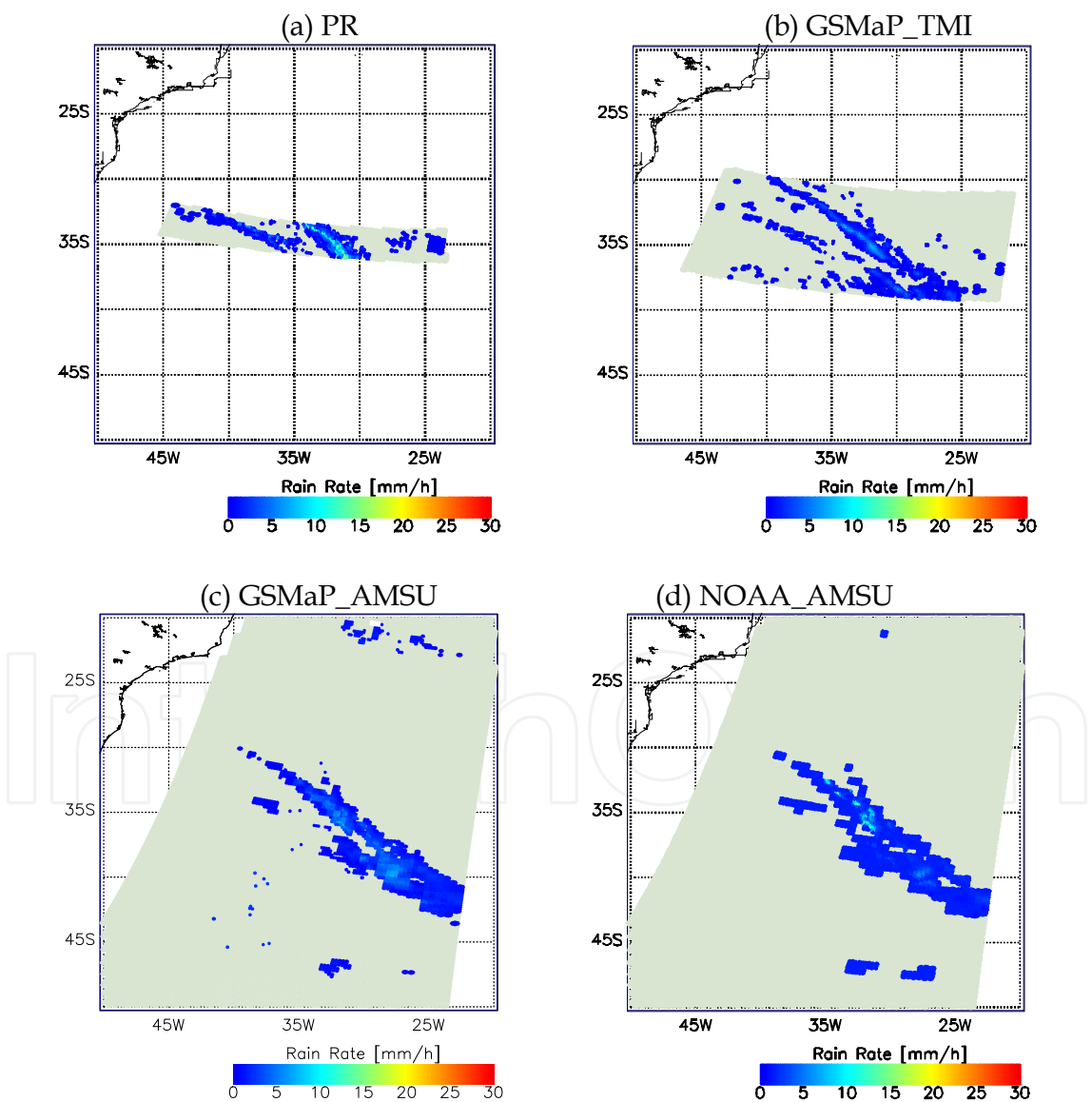
Fig. 2. Rain-rate maps from PR (a), GSMaP_TMI (b) and GSMaP_AMSU (c) for the matched TRMM and NOAA-15(NK) case on 25 July 2005.
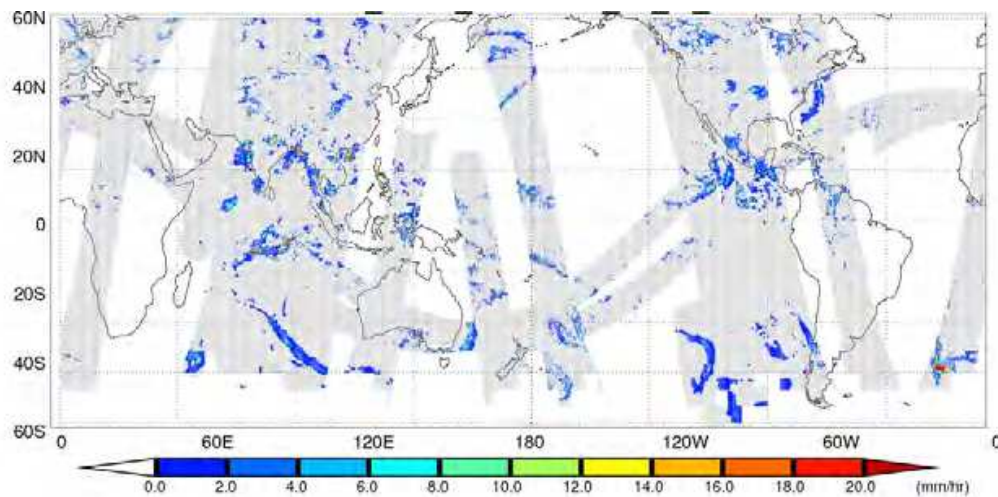
Fig. 3. Combined microwave precipitation estimate at $0.1° \times 0.1°$ for the 3-h period centered at 0130 UTC 25 July 2005 in mm h^{-1} from the TMI, SSM/I, and AMSR-E. Whited-out areas denote regions that lack reliable estimates. (TMI, SSM/I, and AMSR-E are averaged where overlaps occur.)
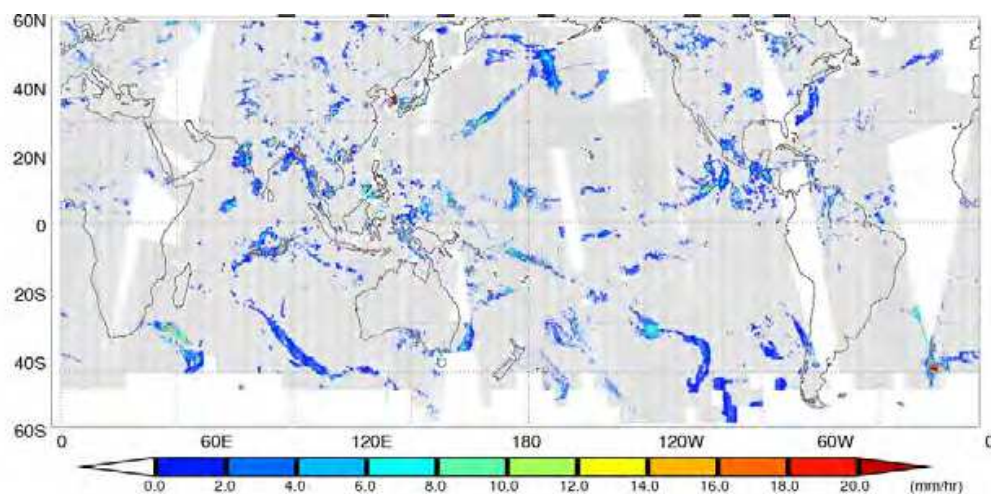

Fig. 4. Same as Fig. 3, but for combined microwave precipitation estimate from the TMI, SSM/I, AMSR-E and AMSU. (TMI, SSM/I, AMSR-E, and AMSU are averaged where overlaps occur.)

4. Discussion and Future Work

As already noted, rainfall retrievals using data from MWIs such as TMI are superior to those using data from MWSs such as AMSU. Figure 5 compares GSMaP_TMI-retrieved and GSMaP_AMSU-retrieved rain rates at $0.1° \times 0.1°$ with rain rates estimated from the ground-based radar at Kwajalein Island, Republic of the Marshall Islands (Wolff et al. 2005). Although it is hard to tell whether the pattern of the GSMaP_TMI rain rates is biased with respect to the Kwajalein radar estimated-rain rates, the GSMaP_AMSU algorithm clearly overestimates (underestimates) rainfall at light (heavy) rain rates. While the TMI scan at a

constant slant path angle, the AMSU radiometer uses cross-track scanning to view the Earth, resulting in the variations in the size of individual FOVs. This variation may lead to less agreement with KR-estimated rain and should be corrected.

Both the GSMaP_MWI and GSMaP_MWS algorithms have been developed using information obtained by the TRMM PR in the latitude band 35oN-35oS. Therefore, uncertainties should be large in the regions where the TRMM PR data is unavailable. The upcoming Global Precipitation Measurement (GPM) core satellite will carry dual-wavelength precipitation radar (DPR) with Ku/Ka–band (13.6/35.5 GHz) and cover the latitude band 65oN-65oS (Senbokuya et al. 2004). Information obtained by the GPM DPR will be used to improve precipitation estimates in the future.

Recently, a new type of MWR suitable for precipitation retrieval and temperature and moisture sounding, such as the Special Sensor Microwave Imager-Sounder (SSMIS; Kunkee et al. 2008), has been carried by satellites. The GPM Microwave Imager, which will be carried by the GPM core satellite together with DPR, also will employ 166 GHz and 183.31 GHz band channels in addition to channels suitable for monitoring precipitation. Thus, it is important to develop the GSMaP algorithm for this type of MWRs.
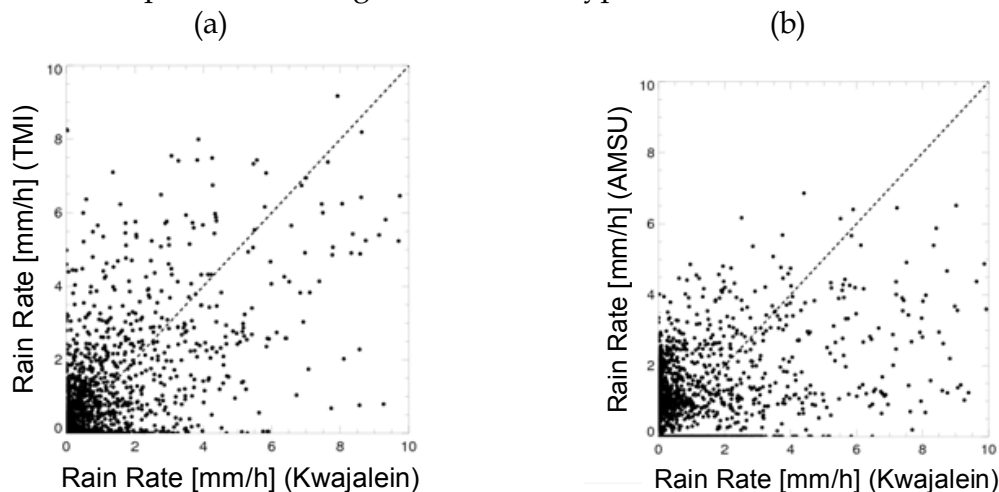
(a)   (b)

Fig. 5. Scatterplots comparing (a) GSMaP_TMI-retrieved and (b) GSMaP_AMSU-retrieved rain rates to KR-estimated rain rates at $0.1° \times 0.1°$. Dashed line shows 1:1 relation.

5. Acknowledgements

6. References

Aonashi, K.; Awaka, J.; Hirose, M.; Kozu, T.; Kubota, T.; Liu, G.; Shige, S.; Kida, S.; Seto, S.; Takahashi, N. & Takayabu, Y. N. (2009). GSMaP passive microwave precipitation retrieval algorithm: algorithm description and validation, *J. Meteor. Soc. Japan*, vol. 87A, pp. 119–136.

Arkin, P. A. & Meisner, B. N. (1987). The relationship between largescale convective rainfall and cold cloud over the Western Hemisphere during 1982–84. *Mon. Wea. Rev.*vol. 115, pp. 51-74.

Colton, M. C. & Poe, G. A. (1999). Intersensor calibration of DMSP SSM/I's: F-8 to F-14, 1987–1997, *IEEE Trans. Geosci. Remote Sens.*, vol. 37, no. 1, pp. 418–439.

Comiso, J. C. (2009). Enhanced sea ice concentrations and ice events from AMSR-E data, *J. Remote Sens. Soc. Japan*, vol. 29, no. 1, pp. 195-215.

Ferraro, R. F.; Weng, F.; Grody, N.; Zhao, L.; Meng, H.; Kongoli, C.; Pellegrino, P.; Qiu, S. & Dean, C. (2005). NOAA operational hydrological products derived from the Advanced Microwave Sounding Unit (AMSU), *IEEE Trans. Geosci. Remote Sens.*, vol. 43, no. 5, pp. 1036–1049.

Grody, N.; Zhao, J.; Ferraro, R.; Weng, F. & Boers, R. (2001). Determination of precipitable water and cloud liquid water over oceans from the NOAA 15 Advanced Microwave Sounding Unit, *J. Geophys. Res.*, vol. 106, no. D3, pp. 2943–2954, 10.1029/2000JD900616.

Guillou, C.; Ellison, W.; Eymard, L.; Lamkaouchi, K.; Prigent, C; Delbos, G.; Balana, G. & Boukabara, S. A. (1998). Impact of new permittivity measurements on sea surface emissivity modeling in microwaves, *Radio Sci.*, vol. 33, no. 3, pp. 649–667.

Hollinger, J. P.; Peirce, J. L. & Poe, G. A. (1990). SSM/I instrument evaluation, IEEE Trans. Geosci. Remote Sens., vol. 28, no. 5, pp. 781–790.

Huffman, G.; Adler, R.; Bolvin, D.; Gu, G.; Nelkin, E.; Bowman, K.; Hong, Y.; Stocker, E. & Wolff, D. (2007). The TRMM Multisatellite Precipitation Analysis (TMPA): Quasi-global, multiyear, combined-sensor precipitation estimates at fine scales, *J. Hydrometeorol.*, vol. 8, no. 1, pp. 38–55.

Iguchi, T.; Kozu, T.; Meneghini, R.; Awaka, J. & Okamoto, K. (2000). Rain profiling algorithm for the TRMM precipitation radar, *J. Appl. Meteorol.*, vol. 39, no. 12, pp. 2038–2052.

Iguchi, T. (2007). Spaceborne radar algorithms, in *Measuring Precipitation From Space – EURAINSAT and the Future*, V. Levizzani, P. Bauer, and F. J. Turk, Eds. New York: Springer-Verlag, pp. 199–212, 2007.

Iguchi, T.; Kozu, T.; Kwiatkowski, J; T.; Meneghini, R.; Awaka, J. & Okamoto, K. (2009). Uncertainties in the rain profiling algorithm for the TRMM precipitation radar, J. Meteorol. Soc. Japan, vol. 87A, pp. 1–30.

Joyce, R. J. ; Janowiak, J. E.; Arkin, P. A. & Xie, P. (2004). CMORPH: A method that produces global precipitation estimates from passive microwave and infrared data at high spatial and temporal resolution, *J. Hydrometeorol.*, vol. 5, no. 3, pp. 487–503.

Kawanishi, T.; Sezai, T.; Ito, Y; Imaoka, K.; Takeshima, T.; Ishido, Y.; Shibata, A.; Miura, M.; Inahata, H. & Spencer, R. W. (2003). The Advanced Microwave Scanning Radiometer for the Earth Observing System (AMSR-E), NASDA's contribution to the EOS for global energy and water cycle studies, *IEEE Trans. Geosci. Remote Sens.*, vol. 41, no. 2, pp. 184–194.

Kozu, T.; Kawanishi, T.; Kuroiwa, H.; Kojima, M.; Oikawa, K.; Kumagai, H.; Okamoto, K.; Okumura, M.; Nakatsuka, H. & Nishikawa, K. (2001). Development of precipitation radar onboard the Tropical Rainfall Measuring Mission satellite, *IEEE Trans. Geosci. Remote Sens.*, vol. 39, no. 1, pp. 102–116.

Kozu, T.; Iguchi, T.; Kubota, T.; Yoshida, N.; Seto, S.; Kwiatkowski, J. & Takayabu, Y. N. (2009). Feasibility of raindrop size distribution parameter estimation with TRMM precipitation radar, *J. Meteorol. Soc. Japan*, vol. 87A, pp. 53–66.

Kubota, T.; Shige, S.; Hashizume, H.; Aonashi, K.; Takahashi, N.; Seto, S.; Hirose, M.; Takayabu, Y. N.; Nakagawa, K.; Iwanami, K.; Ushio, T.; Kachi, M. & Okamoto, K. (2007). Global precipitation map using satelliteborne microwave radiometers by the GSMaP project: Production and validation, *IEEE Trans. Geosci. Remote Sens.*, vol. 45, no. 7, pp. 2259–2275.

Kubota, T.; Ushio T.; Shige S.; Kida S.; Kachi, M. & Okamoto K. (2009). Verification of high resolution satellite-based rainfall estimates around Japan using gauge-calibrated ground radar dataset. *J. Meteor. Soc. Japan*, vol. 87A, pp. 203-222.

Kummerow, C.; Barnes W.; Kozu T.; Shiue J. & Simpson J. (1998). The Tropical Rainfall Measuring Mission (TRMM) sensor package, *J. Atmos. Ocean. Technol.*, vol. 15, no. 3, pp. 809–817.

Kummerow, C.; Olson, W. S. & Giglio, L. (1996). A simplified scheme for obtaining precipitation and vertical hydrometeor profiles from passive microwave sensors, *IEEE Trans. Geosci. Remote Sens.*, vol. 34, no. 5, pp. 1213–1232.

Kummerow, C. D.; Hong, Y.; Olson, W. S.; Yang, S.; Adler, R. F.; McCollum, J.; Ferraro, R.; Petty, G.; Shin, D. B. & Wilheit, T. T. (2001). The evolution of the Goddard profiling algorithm (GPROF) for rainfall estimation from passive microwave sensors, *J. Appl. Meteorol.*, vol. 40, no. 11, pp. 1801–1820.

Kummerow, C.; Masunaga, H. & Bauer, P. (2007). A next-generation microwave rainfall retrieval algorithm for use by TRMM and GPM, in *Measuring Precipitation From Space—EURAINSAT and the Future*, V. Levizzani, P. Bauer, and F. J. Turk, Eds. New York: Springer-Verlag, pp. 235–252, 2007.

Kunkee, D. B.; Poe, G. A.; Boucher, D. J.; Swadley, S. D.; Hong, Y.; Wessel, J. E. & Uliana, E. A. (2008). Design and evaluation of the first Special Sensor Microwave Imager/Sounder, *IEEE Trans. Geosci. Remote Sens.*, vol. 46, no. 4, pp. 863–883.

Liu, G. (1996). A fast and accurate model for microwave radiance calculation, *J. Meteorol. Soc. Japan*, vol. 76, no. 2, pp. 335–343.

Mo, T. (1996). Prelaunch calibration of the Advanced Microwave Sounding Unit-A for NOAA-K, *IEEE Trans. Microw. Theory Tech.*, vol. 44, no. 8, pp. 1460–1469.

Nishitsuji, A.; Hoshiyama, M.; Awaka, J. & Furuhama, Y. (1983). An analysis of propagative character at 34.5 GHz and 11.5 GHz between ETS-II satellite and Kasima station—On the precipitation model from stratus, *IEICE Trans. Commun.*, vol. J66-B, no. 9, pp. 1163–1170, (in Japanese).

Okamoto, K. (2003). A short history of the TRMM precipitation radar, *Meteorol. Monogr.*, vol. 29, no. 51, pp. 187–195.

Okamoto, K. & Shige, S. (2008). TRMM precipitation radar and its observation results, *IEICE Trans. Commun.*, vol. J91-B, no. 7, pp. 723–733, (in Japanese).

Olson, W. S.; Kummerow, C. D.; Song, Y.; Petty, G. W.; Tao, W.-K.; Bell, T. L.; Braun, S. A.; Yansen, W.; Lang, S. E.; Johnson, D. E. & Chiu, C. (2006). Precipitation and latent heating distributions from satellite passive microwave radiometry. Part I: Improved method and uncertainty estimates, *J. Appl. Meteorol. Climatol.*, vol. 45, no. 5, pp. 702–720.

Saunders, R. W.; Hewison, T. J.; Stringer, S. J.; & Atkinson, N. C. (1995). The radiometric characterization of AMSU-B, *IEEE Trans. Microw. Theory Tech.*, vol. 43, no. 4, pp. 760–771.

Schluessel, P. & Luthardt, H. (1991). Surface wind speeds over the North Sea from special sensor microwave/imager observations, *J. Geophys. Res.*, vol. 96, no. C3, pp. 4845–4853.

Senbokuya Y.; Satoh S; Furukawa K; Kojima M; Hanado H; Takahashi N; Iguchi T. & Nakamura K. (2004). Development of the spaceborne dual-frequency precipitation radar for the Global Precipitation Measurement. IGARSS '04, 5, pp. 3566-3569.

Shige, S.; Yamamoto, T.; Tsukiyama, T.; Kida, S.; Ashiwake, H.; Kubota, T.; Seto, S.; Aonashi, K. & Okamoto, K. (2009). The GSMaP precipitation retrieval algorithm for microwave sounders. Part I: Over-ocean algorithm. *IEEE Trans. Geosci. Remote Sens.*, vol. 47, No. 9, pp. 3084-3097.

Simpson, J.; Adler, R. F. & North, G. R. (1988). A proposed satellite Tropical Rainfall Measuring Mission (TRMM). *Bull. Amer. Meteor. Soc.*, vol. 69, no. 3, pp. 278–295

Simpson, J.; Adler, R. F.; Kummerow, C.; W.-K. Tao & R. F. Adler, 1996: On the Tropical Rainfall Measuring Mission (TRMM). *Meteor. Atmos.Phys.*, vol. 60, pp., 19–36.

Surussavadee, C. & Staelin, D. H. (2008a). Global millimeter-wave precipitation retrievals trained with a cloud-resolving numerical weather-prediction model. Part I: Retrieval design, *IEEE Trans. Geosci. Remote Sens.*, vol. 46, no. 1, pp. 99–108.

Surussavadee, C. & Staelin, D. H. (2008b). Global millimeter-wave precipitation retrievals trained with a cloud-resolving numerical weather-prediction model. Part II: Performance evaluation, *IEEE Trans. Geosci. Remote Sens.*, vol. 46, no. 1, pp. 109–118.

Takahashi N. & Awaka, J. (2005). Introduction of a melting layer model to a rain retrieval algorithm for microwave radiometers, in *Proc. 25th IGARSS*, pp. 3404–3409.

Takayabu Y. N. & Katayama, M. (2004). Low-latitudes rainfall characteristics and its meteorological factors analyzed with mesoscale statistics of TRMM PR data, presented at the 1st AOGS, Singapore, Paper 57-OOA-A1683.

Takayabu, Y. N. (2006). Rain-yield per flash calculated from TRMM PR and LIS data and its relationship to the contribution of tall convective rain, *Geophys. Res. Lett.*, vol. 33, No. 18, p. L18705, DOI:10.1029/2006GL027531.

Takayabu, Y. N. (2008). Observing rainfall regimes using TRMM PR and LIS data, *GEWEX News*, vol. 18, no.2, pp. 9-10.

Vila, D.; Ferraro, R. & Joyce, R. (2007). Evaluation and improvement of AMSU precipitation retrievals, *J. Geophys. Res.*, vol. 112, no. D20, p. D20119, DOI: 10.1029/2007JD008617.

Viltard, N.; Burland, C. & Kummerow, C. (2006). Rain retrieval from TMI brightness temperature measurements using a PR-based database, *J. Appl. Meteor. and Climatol.*, vol. 45, pp. 455-466.

Wilheit, T.; Kummerow, C. D. & Ferraro, R. (2003). Rainfall algorithms for AMSR-E, *IEEE Trans. Geosci. Remote Sens.*, vol. 41, no. 2, pp. 204–214.

Wolff, D. B., Marks, D. A.; Amitai, E.; Silberstein, D. S.; Fisher, B. L.; Tokay, A.; Wang, J. & Pippitt, J. L. (2005). Ground validation for the Tropical Rainfall Measuring Mission (TRMM). *J. Atmos. Oceanic Technol.*, vol. 22, No. 4, pp. 365–380.
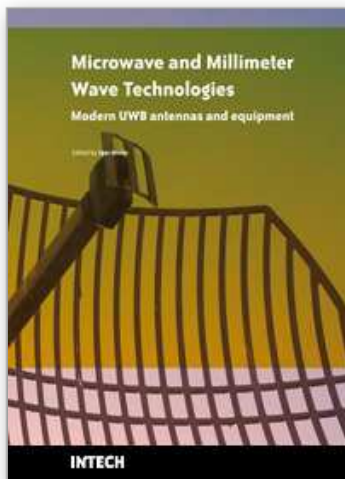
Microwave and Millimeter Wave Technologies Modern UWB antennas and equipment

Edited by Igor Mini

How to reference

In order to correctly reference this scholarly work, feel free to copy and paste the following:

INTECH
open science | open minds